Archive of Applied Mechanics 72 (2003) 715 – 729 © Springer-Verlag 2003
DOI 10.1007/s00419-002-0255-4

Thermal stresses and shakedown in wheel/rail contact

M. Ertz, K. Knothe

Summary Sliding friction between railway wheels and rails results in considerable contact temperatures and gives rise to severe thermal stresses at the surfaces of the wheels and rails. An approximate analytical solution is presented for a line contact model. The increased bulk temperature of the wheel after a long period of constant operating conditions is also taken into account. The thermal stresses have to be superimposed on the mechanical contact stresses. They reduce the elastic limit of the wheel and rail, and yielding begins at lower mechanical loads. When residual stresses build up during the initial cycles of plastic deformation, the structure can carry higher loads with a purely elastic response in subsequent load cycles. This phenomenon is referred to as shakedown. Due to the distribution of temperature, the rail surface is generally subjected to higher stresses than the wheel surface. This can cause structural changes in the rail material and hence rail damage.

Keywords Wheel/rail system, Contact temperature, Thermal stress, Shakedown

1 Introduction

The contact area between a train wheel and a rail has barely the size of a thumbnail. Stresses in this area are amongst the highest known in engineering, even if only the mechanical load due to the axle static load and tractive forces is considered. The classical approach to the calculation of mechanical contact stresses is based on the theory of Hertz [1]. The problem of the rolling contact was investigated in detail by Johnson. For his first studies, he used the two-dimensional model of a line contact of an infinite cylinder subjected to normal and tangential loads, [2]. In the case of full sliding, the stress field depends here only on the maximum Hertz pressure p_0 and on the coefficient of friction μ. The critical value of p_0 at the onset of yielding is called in this context the elastic limit and it can be calculated as a function of μ. For purely normal load ($\mu = 0$), the state of stress at the surface is nearly hydrostatic and first yielding occurs at a point beneath the surface. Due to the tangential traction, the surface stresses increase, and for $\mu > 0.3$ the first yielding occurs at the surface, [3].

During the initial cycles of plastic deformation, residual stresses build up. This increases the elastic limit, i.e. the structure can carry higher loads, while remaining within the purely elastic behaviour in subsequent load cycles due to the superimposed residual stresses. The maximum value of p_0 at the onset of yield in the presence of residual stresses is called the shakedown limit.

Although shakedown is a process including plastic deformation, no elastic–plastic analysis is required to obtain the shakedown limit. Following the approach of Melan, [4], one has to find a system of residual stresses that keeps the resulting stresses within the yield limit. This requires only a number of purely elastic calculations with a variation of residual stresses. If the shakedown limit is exceeded, repeated plastic deformation will take place within every load cycle, [5]. This will cause eventually crack initiation and an early failure, [6]. Elastic limit and shakedown limit can easily be plotted in shakedown maps, Fig. 1, which have been introduced in [3]. The case of partial slip and the contact of spherical bodies with an elliptical area of contact was also studied in [3]. Johnson's approach is still widely used in today's railway

Received 7 May 2002; accepted for publication 3 September 2002

M. Ertz (✉), K. Knothe
Technische Universität Berlin, Sekr. F5, Marchstr. 12,
D-10587 Berlin, Germany
e-mail: martin.ertz@tu-berlin.de

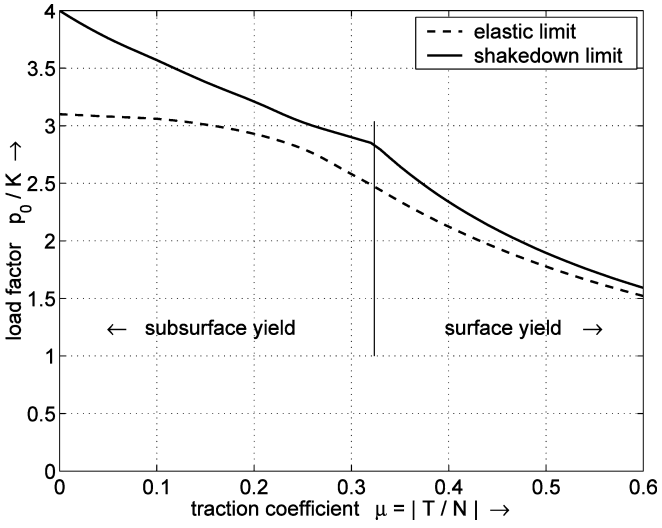

Fig. 1. Shakedown map – the effect of tangential traction on the elastic limit and on the shakedown limit, according to the yield criterion of von Mises, [3]. (p_0^-: maximum Hertz pressure, K^-: yielding shear stress)

engineering, [6]. His results were compared with a full elastic–plastic analysis of a plane strain model, [7, 8]. The finite element calculations validated the basic assumptions made in [5]. Although the investigation revealed significant differences in the amount and distribution of residual stress and strain components, shakedown was observed at similar loads.

Thermal stresses can also contribute to plastic flow and failure in rolling and sliding contact. Although sliding is always connected with increased temperatures and thermal stresses, these have not been included in Johnson's investigations. Their order of magnitude depends additionally on the physical parameters, like: the size of the contact patch, the sliding velocity v_s and vehicle speed v_0, the thermal expansion coefficient α and the elastic properties, as well as the heat conduction properties.

It has been shown in a number of investigations that thermal stresses in railway wheels and rails can be of the same order of magnitude as the stresses due to mechanical loading. Severe stresses in wheels are caused by the nonuniform heating, which results from tread braking, [9–11]. The heating due to the sliding in a wheel/rail contact and the associated thermal stresses were calculated in [12]. The problem was simplified by assuming full axial symmetry of the wheel. Thus, the stress field in the cross section of the wheel due to the increasing bulk temperature could be investigated quite efficiently, but the high temperature changes due to the periodic contact of the wheel tread with the brake shoe or the rail were neglected. Investigations of thermal contact stresses have been carried out also in [13–15].

Some recent results of the shakedown analysis including thermal stresses have been given in [16, 17]. The yield conditions used were more general than those in Johnson's works, but problems of rolling or sliding contact were not investigated. Since the focus of the present paper is not on the shakedown theory or material behaviour, but rather on the principal effects of thermal stresses in the wheel/rail contact, we will use the most simple model of elastic-ideal plastic material that has also been assumed in the first works of Johnson.

2
Mechanical contact

When a wheel and rail are brought into contact under the action of the static wheel load, the area of contact and the pressure distribution are usually calculated by the Hertz theory. In this case, the area of contact is elliptical and the normal pressure distribution is, [1, 18],

$$p_z(x,y) = p_0\sqrt{1-\frac{x^2}{a^2}-\frac{y^2}{b^2}}\ , \tag{1}$$

with the maximum pressure given by

$$p_0 = \frac{3N}{2\pi ab}\ , \tag{2}$$

where the normal load is N and the semi-axes of the contact ellipse are a (in the rolling direction) and b. If one is only interested in the maximum stresses and contact temperatures that occur at $y = 0$, the two-dimensional model of an infinite cylinder subjected to normal and tangential loading (called line contact) is often used for a simplified analysis, Fig. 2. Here we have a state of plane strain with $\tau_{xy} = \tau_{yz} = 0$, Fig. 3. The values of a and p_0 have to be taken from the three-dimensional problem. If the contact occurs at the rail tread, the lateral width $2b$ of the ellipse is usually larger than the length $2a$, and the contact pressure near the centre of the ellipse changes only slightly with y. In this case, the two-dimensional model provides a good approximation, but it should not be used in flange contact with $a \geq b$.

In the case of full sliding, the ratio of the tangential force T and the normal load N is equal to the coefficient of friction μ, which is assumed to be constant within the area of contact. With the non-dimensional coordinate $\xi = x/a$, the stresses at the contact surface due to both the pressure and the tangential traction can be written as, [18],

$$\sigma_x = -p_0\left(\sqrt{1-\xi^2} \pm 2\mu\xi\right) \ , \tag{3}$$

$$\sigma_z = -p_0\sqrt{1-\xi^2} \ , \tag{4}$$

$$\tau_{xz} = \mp\mu p_0\sqrt{1-\xi^2} \ . \tag{5}$$

Outside the area of contact ($|\xi| > 1$), σ_z and τ_{xz} are zero and the normal stress in longitudinal direction is

$$\sigma_x = \mp 2\mu p_0\left[\xi - \mathrm{sgn}(\xi).\sqrt{\xi^2-1}\right] \ . \tag{6}$$

For the state of plane strain, the normal stress in lateral direction is always

$$\sigma_y = v(\sigma_x + \sigma_z) \ , \tag{7}$$

with Poisson's ratio v. The sign of the tangential stress τ_{xz} in Eq. (5) and of the part of σ_x due to tangential loading in Eqs. (3) and (6) is different for driving and braking. The upper sign refers to the wheel in the case of braking and to the rail in the case of driving, whereas the lower sign refers to the wheel in the case of driving and to the rail in the case of braking, Fig. 3.

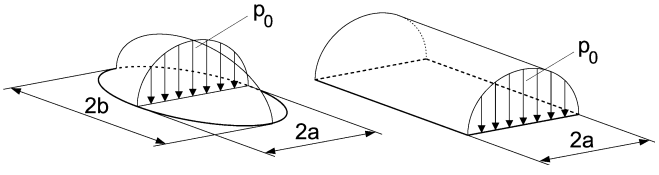

Fig. 2. Normal pressure distribution in a three- and a two-dimensional contact

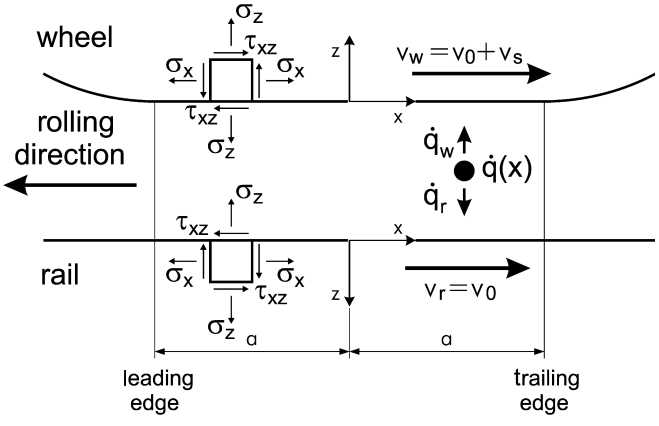

Fig. 3. Coordinate systems for the calculation of temperatures and stresses in the wheel/rail contact

3
Contact temperature

3.1
Frictional heating

The power dissipation due to tangential stress and sliding velocity between wheel and rail results in contact temperatures that can exceed 200 °C under normal operating conditions. They are confined to a very thin surface layer. The thermal penetration depth

$$\delta = \frac{a}{\sqrt{\mathrm{L}}} \ , \tag{8}$$

depends on the non-dimensional Péclet number

$$L = \frac{av}{2\kappa} \ , \tag{9}$$

with the semi-axis length a, the speed v of the moving heat source and the thermal diffusivity

$$\kappa = \frac{\lambda}{\varrho c} \ , \tag{10}$$

that combines the material properties λ (thermal conductivity), ϱ (density) and c (specific heat capacity), [18, 19]. If $L > 10$, heat conduction occurs only perpendicular to the contact plane, i.e. in the z-direction, [19]. With the typical values for the wheel/rail contact, $a \approx 5$ mm, $\kappa = 14.2 \times 10^{-6}$ m^2/s, [12], and $v_0 = 30$ m/s, one gets $L \approx 5000$. Thus the longitudinal and lateral heat conduction (in the x- and y-directions) can be neglected and the thermal penetration depth is only $\delta \approx 0.015a$ for these parameters.

High contact temperatures occur at high values of the sliding velocity v_s. In this case, elastic deformations of the wheel and rail can be neglected and the distribution of frictional heating for Hertzian contact is

$$\dot{q}_\mathrm{friction} = \mu |v_\mathrm{s}| p_z(\xi) = \mu |v_\mathrm{s}| p_0 \sqrt{1 - \xi^2} \ . \tag{11}$$

It is generally assumed that the dissipated frictional power is completely transformed into heat. The heat flows into the material of the wheel and rail. With equal thermal properties of the wheel and rail, the heat partitioning factor depends only slightly on the different velocities of wheel and rail with respect to the area of contact, Fig. 3. For reasons of simplicity, we will assume equal partitioning of the heat into the wheel and rail in the following. Compared with the exact solution, [20], the error is always less than 5% for typical operating conditions in the wheel/rail contact.

The surface temperature due to the Hertz distribution of frictional heating can be calculated by means of a polynomial approximation as

$$\Theta_w(\xi) = \Theta_\Gamma(\xi) = \mu p_0 |v_\mathrm{s}| \sqrt{\frac{a}{\lambda \varrho c v_0}} f_1(\xi) \ , \tag{12}$$

with the non-dimensional function

$$f_1(\xi) = \frac{\sqrt{\pi}}{256} \times \begin{cases} 0 & \text{for } \xi < -1, \\ \sqrt{\xi + 1}(71 + 12\xi - 20\xi^2 + 8\xi^3 - 16\xi^4) & \text{for } |\xi| \le 1, \\ \sqrt{\xi + 1}(71 + 12\xi - 20\xi^2 + 8\xi^3 - 16\xi^4) & \\ \quad - \sqrt{\xi - 1}(71 - 12\xi - 20\xi^2 - 8\xi^3 - 16\xi^4) & \text{for } \xi > 1 \ , \end{cases} \tag{13}$$

given in [20]. The result is shown in Fig. 4. The zero-point of temperature can be conveniently chosen as the ambient temperature. Thus, in this paper, Θ always represents the temperature rise due to the heat supplied within the contact patch.

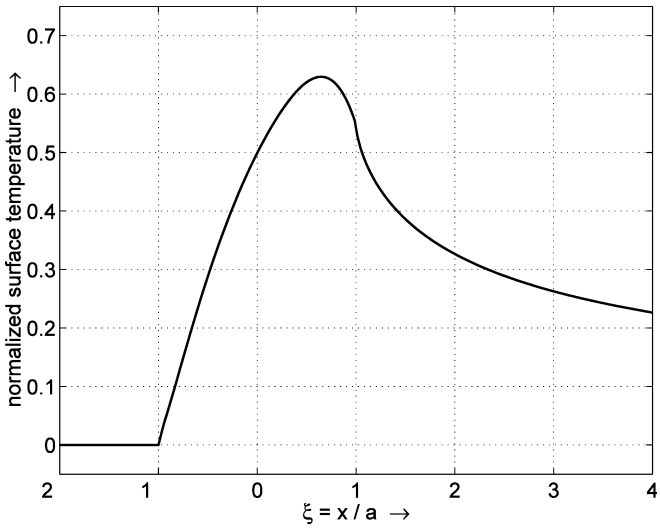

Fig. 4. Surface temperature distribution of wheel and rail due to frictional heating; wheel and rail initially at ambient temperature, normalized with respect to the steady-state wheel temperature Θ_∞, Eq. (14)

The temperature distribution for rolling/sliding contact presented in this section is based on the exact solution of the heat conduction equation for moving heat sources with one-dimensional heat flow in the z-direction. This assumption is justified for fast moving heat sources with very high values of the Péclet number L, Eq. (9). The approach can be extended to the consideration of three-dimensional contact problems (elliptical area of contact) without any restriction, [20]. It is much more efficient than a finite element solution. Since the surfaces of the wheel and rail move with respect to the contact patch, the temperature cannot be obtained from a simple stationary heat conduction calculation. Either a transient calculation with very small time increments or the concept of ALE (Arbitrary Eulerian–Lagrangian) relative kinematics, [21], would be required for the adequate treatment of the problem. Additionally, the discretisation should be extremely fine in the z-direction due to the very small thermal penetration depth δ.

3.2
Initial wheel temperature

The bulk temperature of the wheel increases over time due to the periodical frictional heating at its surface, [12]. Therefore the temperatures of the wheel and the rail are different when a point at the surface of the wheel comes into the area of contact again. This can be treated approximately as the contact of two semi-infinite bodies with different initial temperatures, [22]. Upon coming into contact, a constant surface temperature is reached immediately. With equal thermal properties of the wheel and the rail, it is the mean value of their initial temperatures. The contact of two bodies with different initial temperatures gives rise to heat conduction from the hot wheel into the cold rail through the contact patch. Since the heat loss due to conduction into the rail is proportional to the difference in surface temperatures, it will be equal to the frictional heating at a value of the initial wheel temperature that can be calculated as

$$\Theta_\infty = \mu p_0 |v_s| \sqrt{\frac{\pi^3 a}{32 \lambda \varrho c v_0}} \ , \tag{14}$$

from a simple energy balance, [20]. Thus all the frictional heating flows into the rail while the wheel temperature remains constant. This temperature is the upper limit for constant operating conditions. It is approximately twice the average surface temperature in the case of an initially cold wheel, Fig. 5. Convection on the circumference of the cylinder can be neglected in the case of line contact. For real wheels, the steady-state temperature is lower due to convection over the whole surface of the wheel, [20]. The subscript ∞ in Eq. (14) indicates that a steady-state temperature will only be reached after a very long operating time, e.g. 60–120 min for a real wheel, considering convection, [23]. Usually, the increased bulk temperature Θ_0 of the wheel will be between 0 and Θ_∞. It is meaningful to introduce the non-dimensional temperature

$$\tilde{\Theta}_0 = \frac{\Theta_0}{\Theta_\infty} \ , \tag{15}$$

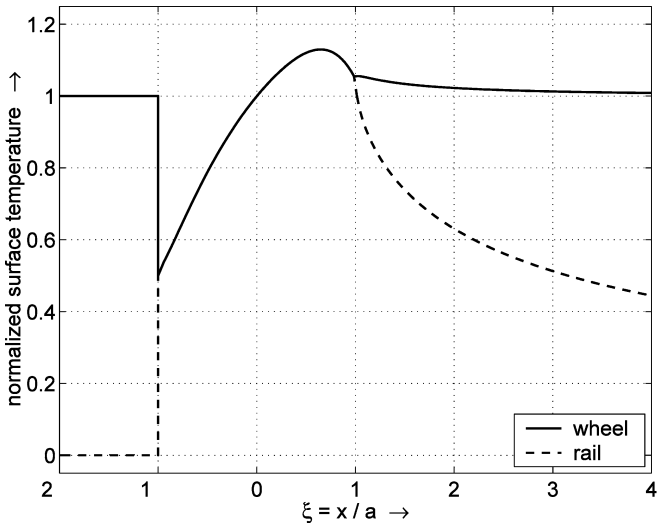

Fig. 5. Surface temperature distribution of wheel and rail due to frictional heating and steady-state initial wheel temperature Θ_∞, normalized with respect to the steady-state wheel temperature Θ_∞, Eq. (14)

called the initial relative temperature of the wheel, with $0 \leq \tilde{\Theta}_0 \leq 1$ for constant operating conditions. Using $\tilde{\Theta}_0$ and the non-dimensional function

$$f_2(\xi) = \sqrt{\frac{\pi^3}{128}} \times \begin{cases} 0 & \text{for } \xi < -1, \\ 1 & \text{for } |\xi| \leq 1, \\ \frac{2}{\pi} \arcsin \sqrt{\frac{2}{\xi+1}} & \text{for } \xi > 1 \ , \end{cases} \tag{16}$$

the surface temperature due to the initial temperature Θ_0 of the wheel can be written for the wheel as

$$\Theta_\mathrm{w}(\xi) = \tilde{\Theta}_0 \mu p_0 |v_\mathrm{s}| \sqrt{\frac{a}{\lambda \varrho c v_0}} \left[\sqrt{\frac{\pi^3}{32}} - f_2(\xi) \right] \ , \tag{17}$$

and

$$\Theta_\mathrm{r}(\xi) = \tilde{\Theta}_0 \mu p_0 |v_\mathrm{s}| \sqrt{\frac{a}{\lambda \varrho c v_0}} f_2(\xi) \ , \tag{18}$$

for the rail, [20, 22].

4
Thermal stresses

The contact temperature gives rise to severe thermal stresses at the surfaces of wheel and rail. An accurate analysis of this problem would only be possible with a finite element model, [14]. But since the large changes in temperature are confined to a very thin surface layer, we can assume that the expansion of the surface in the x- and y-directions is zero while the expansion in the z-direction is possible without restriction. Thus the pure thermal loading results in a state of plane stress parallel to the surface, with $\epsilon_x = 0$, $\epsilon_y = 0$ and $\sigma_z = 0$. The thermal stresses are

$$\sigma_x = \sigma_y = -\frac{E\alpha}{1-\nu} \Delta\Theta \ , \tag{19}$$

with the Young's modulus E, the thermal expansion coefficient α and the Poisson's ratio ν. The temperature difference $\Delta\Theta$ between the surface and the bulk material is

$$\Delta\Theta_\mathrm{w}(\xi) = \Theta_\mathrm{w}(\xi) - \Theta_0 \tag{20}$$

for the wheel (initial temperature Θ_0) and

$$\Delta\Theta_\mathrm{r}(\xi) = \Theta_\mathrm{r}(\xi) \tag{21}$$

for the rail (initial temperature 0). If the local surface temperature is higher than the bulk temperature, one obtains compressive stresses at the surface. This approximation has been introduced at first by Schouten, [24]. He compared the results of Eq. (19) with the output of finite element calculations and concluded that the simple approach should be accurate enough for the calculation of thermal stresses in a sliding contact. This was confirmed in [13] where it was stated that the approximation yields good results for fast moving heat sources with a very small thermal penetration depth δ.

Nevertheless, we will try to estimate the error of this approximation in the case of pure frictional heating, with the wheel initially at ambient temperature, Fig. 4. The equilibrium condition for the stresses in the x-direction is

$$\frac{\partial \sigma_x}{\partial x} + \frac{\partial \tau_{xz}}{\partial z} = 0 \ . \tag{22}$$

Since σ_x is not constant, a shear stress τ_{xz} is required for equilibrium. Because the maximum temperature and thermal stress occur near the trailing edge, we obtain

$$\frac{\partial \sigma_x}{\partial x} \approx \frac{\sigma_{x,\max}}{2a} \ , \tag{23}$$

as a rough approximation for the first term in Eq. (22). At the surface, τ_{xz} must disappear. We assume that its maximum occurs beneath the surface within the area of increased temperature (thermal penetration depth δ), and therefore we can approximate the second term as

$$\frac{\partial \tau_{xz}}{\partial z} \approx \frac{\tau_{xz,\max}}{\delta} \ . \tag{24}$$

Combining Eqs. (22)–(24), it follows that

$$\left| \frac{\tau_{xz,\max}}{\sigma_{x,\max}} \right| \approx \frac{\delta}{2a} \approx \frac{1}{2\sqrt{\mathrm{L}}} \ , \tag{25}$$

which is in the range of 1%, see Eqs. (8) and (9). Thus, the error in the thermal stress field should be negligible using the approximate solution. Considering an initial wheel temperature, there is a discontinuity at the leading edge, s. Fig. 5. There, the error has to be expected to be more significant. Fortunately, this point is mostly of minor importance when finding the maximum equivalent stress that will initiate first yield, Figs. 6–9.

Combining Eq. (19) with the approximate solution for the surface temperature in the case of Hertzian contact, s. Sect. 3, the thermal stresses can be written conveniently for the wheel as

$$\sigma_x = \sigma_y = -\mu p_0 \mathrm{J} [\, f_1(\xi) - \tilde{\Theta}_0 f_2(\xi)] \ , \tag{26}$$

and for the rail as

$$\sigma_x = \sigma_y = -\mu p_0 \mathrm{J} [\, f_1(\xi) + \tilde{\Theta}_0 f_2(\xi)] \ . \tag{27}$$

We have introduced here a non-dimensional quantity

$$\mathrm{J} = \frac{E\alpha |v_s|}{1-\nu} \sqrt{\frac{a}{\lambda \varrho c v_0}} \ , \tag{28}$$

which we will call the Johnson number. It combines all influence parameters for the thermal stresses except for the initial relative temperature $\tilde{\Theta}_0$ of the wheel, Eq. (15), i.e. the ratio of the initial wheel temperature Θ_0 to the maximum possible temperature Θ_∞, Eq. (14). As explained before, $0 \le \tilde{\Theta}_0 \le 1$ for constant operating conditions. Functions $f_1(\xi)$ in Eq. (13) and $f_2(\xi)$ in Eq. (16) are non-dimensional functions of ξ that do not depend on physical parameters, [20].

If both the wheel and the rail are initially at the ambient temperature, then their surface contact temperatures and thermal stresses are equal. But when the wheel is initially at Θ_∞, the situation is completely different. It is obvious from Fig. 5 that the local temperature difference

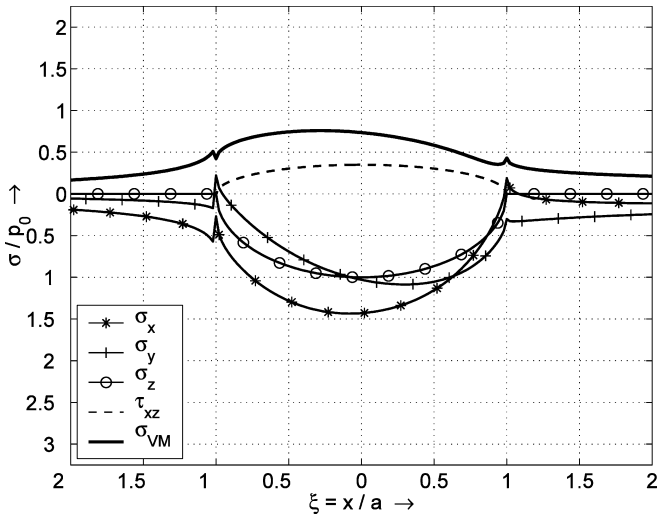

Fig. 6. State of stress at the surface of the wheel, driving with Johnson number J = 5; initial relative wheel temperature $\bar{\Theta}_0 = 0.5$, coefficient of friction $\mu = 0.35$

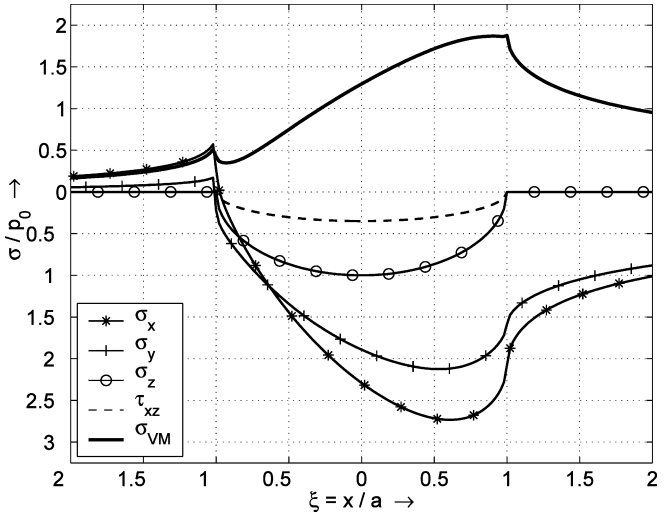

Fig. 7. State of stress at the surface of the rail, driving with Johnson number J = 5; initial relative wheel temperature $\bar{\Theta}_0 = 0.5$, coefficient of friction $\mu = 0.35$

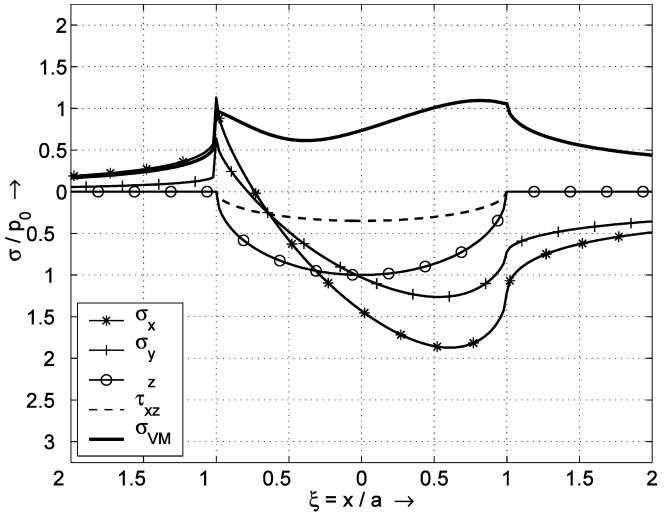

Fig. 8. State of stress at the surface of the wheel, braking with Johnson number J = 5; initial relative wheel temperature $\bar{\Theta}_0 = 0.5$, coefficient of friction $\mu = 0.35$

between surface and bulk material is 50% of Θ_∞ for the wheel and occurs at the leading edge. This is even lower than for $\Theta_0 = 0$. The maximum surface temperature of the rail is approx. 110% of Θ_∞, while the bulk material is still at ambient temperature. Thus the pure thermal

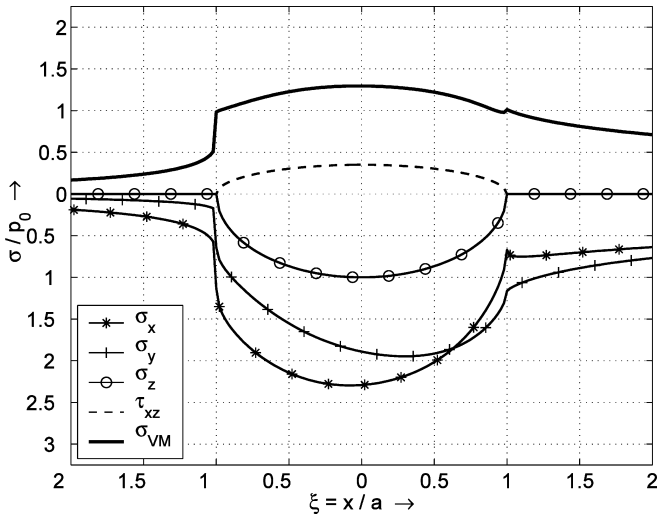

Fig. 9. State of stress at the surface of the rail, braking with Johnson number J = 5; initial relative wheel temperature $\tilde{\Theta}_0 = 0.5$, coefficient of friction $\mu = 0.35$

stresses in the rail are more than twice as high as in the wheel if the wheel temperature has reached the maximum possible value for constant operating conditions.

5
Elastic limit

Yielding begins when the equivalent stress is equal to the yield limit σ_Y. Here, we use the v. Mises yield criterion

$$\sigma_{VM} = \sigma_Y \quad , \tag{29}$$

with the equivalent stress

$$\sigma_{VM} = \frac{1}{\sqrt{2}} \sqrt{(\sigma_x - \sigma_y)^2 + (\sigma_y - \sigma_z)^2 + (\sigma_z - \sigma_x)^2 + 6\tau_{xz}^2} \quad , \tag{30}$$

for a state of plane strain. In simple shear the yield stress is $\sigma_Y = \sqrt{3}K$. Since all components of mechanical and thermal stresses are proportional to p_0, the yield criterion can be used to calculate the maximum Hertz pressure p_0 called the elastic limit at which yielding begins, Fig. 10.

The stresses due to normal loading are equal in the wheel and the rail. For Hertz contact with full sliding, only the sign of the stresses due to tangential loading depends on the direction of the tangential force acting on the wheel and rail, see Eqs. (3), (5) and (6). Without thermal

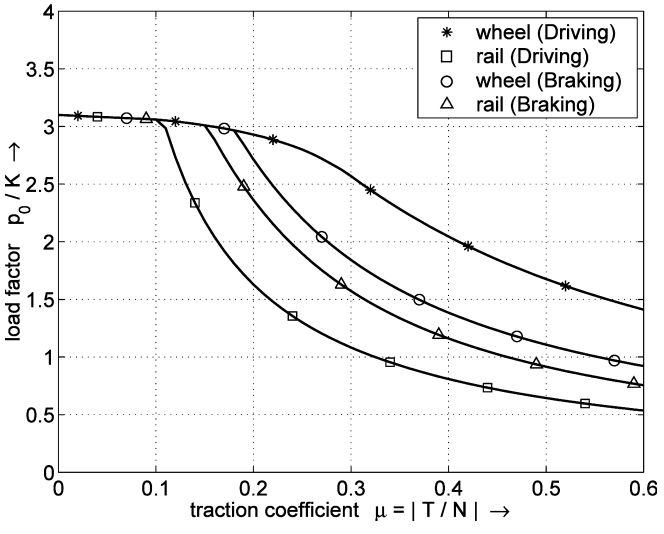

Fig. 10. Effect of the traction coefficient on the elastic limit; Johnson number J = 5, initial relative wheel temperature $\tilde{\Theta}_0 = 0.5$

stresses, the distribution of the equivalent stress in the wheel and the rail is equal, but with reverse orientation. Therefore, it is not necessary to differentiate between the wheel and the rail or between driving and braking, and the yield criterion is the same in all cases, s. Fig. 1.

If the wheel and the rail are initially at the ambient temperature, the thermal stresses due to frictional heating are equal in both of them. But the distribution of equivalent stress is no longer the same in all cases because of the combined mechanical and thermal stresses. On one hand, the results are equal for the wheel in the case of braking and for the rail in the case of driving, and, on the other hand, for the wheel in the case of driving and for the rail in the case of braking. The maximum thermal stresses occur near the trailing edge and are negative (compressive stresses). In this area, the tangential loading also results in compressive stresses for the wheel in the case of braking and for the rail in the case of driving. When mechanical and thermal stresses are superimposed, the resulting equivalent stress is higher than in the other possible combinations (wheel in the case of driving, rail in the case of braking).

If the wheel is initially above ambient temperature, things are even more complicated. Now, thermal stresses are no longer equal in the wheel and the rail, but always higher in the rail, s. Fig. 5. We get these different results for wheel and rail as well as for driving and braking, s. Figs. 6–9. The worst situation is always for the rail in the case of driving and the lowest stresses occur for the wheel in the case of driving. Therefore, we will investigate only these two cases in the following.

6
Residual stresses and the shakedown limit

As already mentioned, if the elastic limit is exceeded during the initial load cycles, plastic deformations occur: after the removal of the external load, residual stresses remain in the wheel and rail. Johnson investigated in [2] the influence of residual stresses on subsequent load cycles, assuming an elastic-ideal plastic material. Based on Melan's theorem, the structure shakes down if there exists any time-independent distribution of residual stresses which together with the elastic stresses due to the external load keeps the stresses within the yield limit. If no such system of stress can be found, then the structure will not shake down and plastic flow will continue within every subsequent load cycle, [4]. The shake down limit is the maximum load (i.e. maximum Hertz pressure p_0) that can be carried elastically in repeated contact after the formation of residual stresses without further plastic flow.

The only possible system of residual stresses for rolling line contact consists of direct stresses $\sigma_{x,R}(z)$ and $\sigma_{y,R}(z)$ parallel to the surface, [2, 3]. This follows from the conditions of

- plane state of strain,
- continuous and steady deformation, and
- traction-free surface.

The stresses $\sigma_{x,R}(z)$ and $\sigma_{y,R}(z)$ have to be varied independently in order to find the minimum of the equivalent stress.

Johnson's approach can easily be extended to the consideration of thermal stresses. Since thermal stresses are restricted to a very thin surface layer, they have only to be considered at the surface ($z = 0$), and the results beneath the surface can be taken from [3] without any modification, s. Fig. 1. For reasons of simplicity, we also assume elastic-ideal plastic behaviour of the material. The residual stresses $\sigma_{x,R}$ and $\sigma_{y,R}$ at the surface are varied by numerical optimization. With an increased initial temperature of the wheel, the results are again different for the wheel and the rail as well as for driving and braking, Fig. 11.

7
Application to the wheel/rail contact

Shakedown maps have been calculated for some values of the non-dimensional Johnson number J both for equal and different initial temperatures of the wheel and rail, Figs. 12–17. Some values of J can be found in Table 1 for usual wheel/rail operating conditions. Typical values of the steady-state wheel temperature Θ_∞ are also given. While the influence of thermal stresses on the elastic limit and shakedown limit can be reduced to the non-dimensional parameters J (the Johnson number) and $\tilde{\Theta}_0$ (the initial relative wheel temperature), contact temperatures depend additionally on the coefficient of friction μ and on the maximum Hertz pressure p_0.

The Johnson number J, Eq. (28), can be in the range of 5–10 for usual operating conditions. Assuming the material parameters to be constant and independent of temperature, J increases

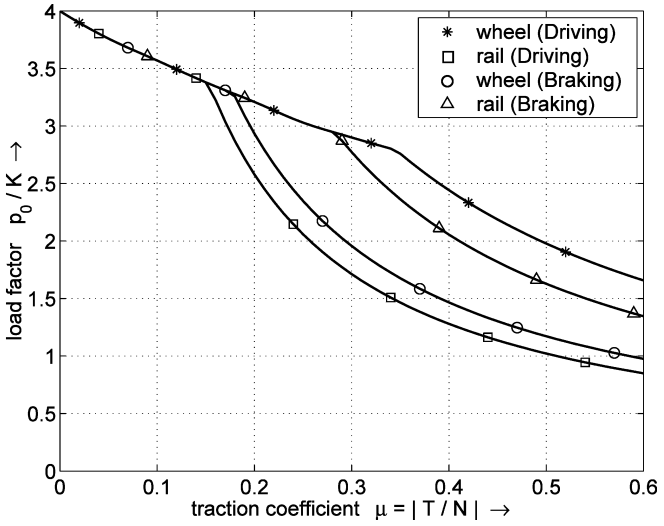

Fig. 11. Effect of the traction coefficient on the shakedown limit; Johnson number $J = 5$, initial relative wheel temperature $\tilde{\Theta}_0 = 0.5$

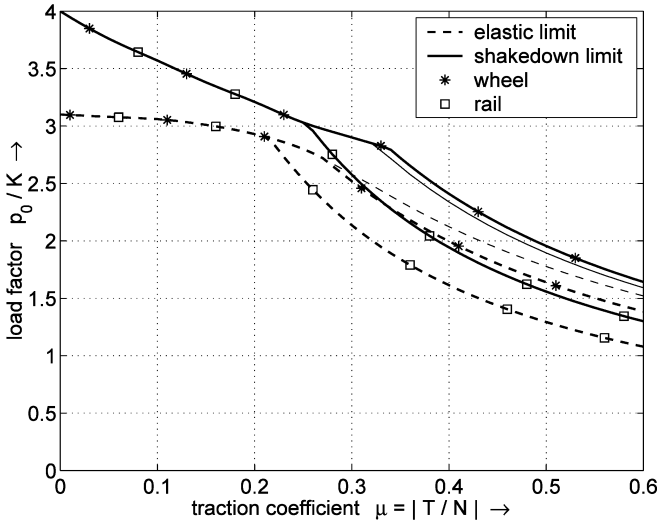

Fig. 12. Shakedown map in the case of driving; Johnson number $J = 2$, initial relative wheel temperature $\tilde{\Theta}_0 = 0$ (faint lines: results without thermal stresses, see also Fig. 1)

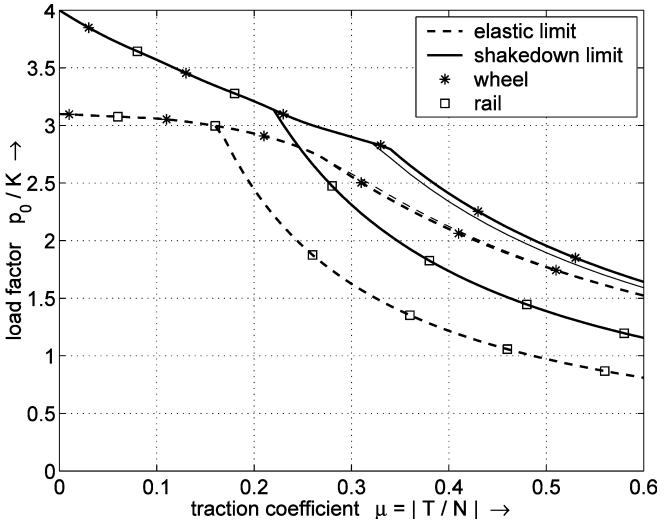

Fig. 13. Shakedown map in the case of driving; Johnson number $J = 2$, initial relative wheel temperature $\tilde{\Theta}_0 = 1$ (faint lines: results without thermal stresses, see also Fig. 1)

with large values of the sliding velocity v_s and of the length a. It diminishes with large values of the vehicle speed v_0. With $J = 5$, there is already a significant influence on the elastic limit and shakedown limit, Figs. 14 and 15. At the same time, the contact temperature is still not high

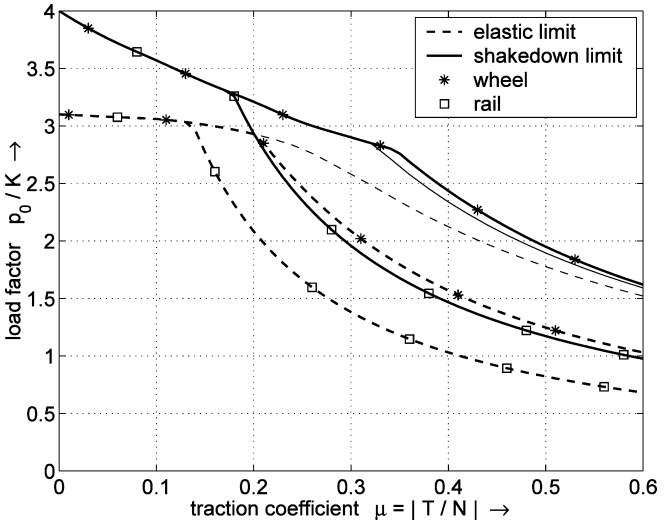

Fig. 14. Shakedown map in the case of driving; Johnson number J = 5, initial relative wheel temperature $\tilde{\Theta}_0 = 0$ (faint lines: results without thermal stresses, see also Fig. 1)

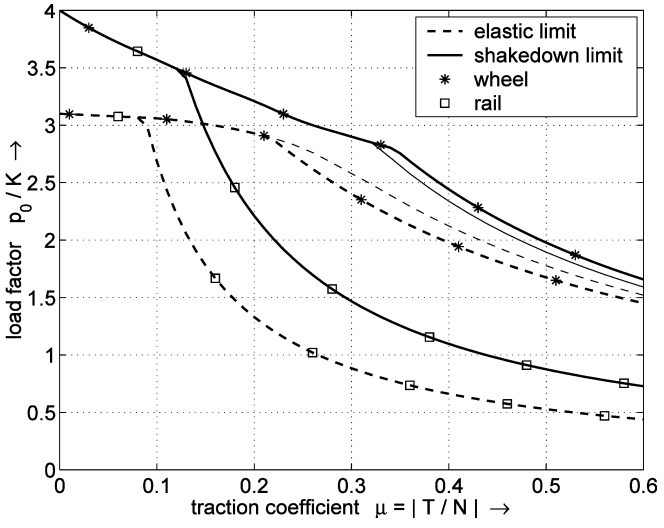

Fig. 15. Shakedown map in the case of driving; Johnson number J = 5, initial relative wheel temperature $\tilde{\Theta}_0 = 1$ (faint lines: results without thermal stresses, see also Fig. 1)

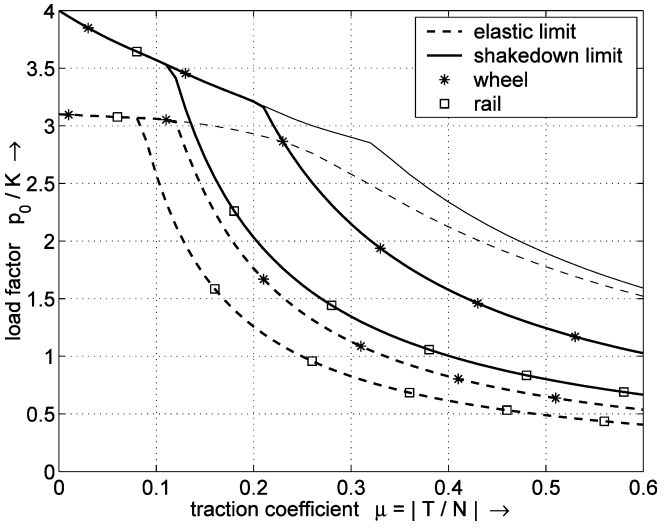

Fig. 16. Shakedown map in the case of driving; Johnson number J = 10, initial relative wheel temperature $\tilde{\Theta}_0 = 0$ (faint lines: results without thermal stresses, see also Fig. 1)

enough to cause thermally induced phase transformations. Consider as a typical example a freight train running with the speed $v_0 = 30$ m/s and the sliding velocity $v_s = 1.3$ m/s (approx. 4.3% creepage). The wheel load of the locomotive is $N = 100$ kN. The semi-axes of the contact

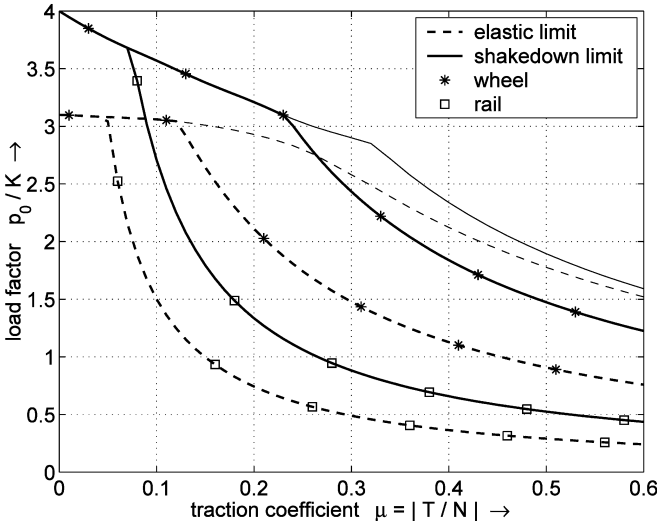

Fig. 17. Shakedown map in the case of driving; Johnson number J = 10, initial relative wheel temperature $\tilde{\Theta}_0 = 1$ (faint lines: results without thermal stresses, see also Fig. 1)

Table 1. Johnson number J, Eq. (28), for different values of the vehicle speed v_0 and sliding velocity v_s ($a = 6$ mm, $E = 2.1 \times 10^5$ MPa, $\alpha = 1.2 \times 10^{-5}$ K^{-1}, $\nu = 0.3$, $\lambda = 50$ W/K m, $\varrho = 7850$ kg/m^3, $c = 450$ J/kg K). The steady-state wheel temperature Θ_∞, Eq. (14), depends additionally on the coefficient of friction μ and on the maximum Hertz pressure p_0; the temperatures in this Table have been calculated for $p_0 = 800$ MPa and the specified values of μ

v_0 [m/s]	v_s [m/s]	J	Θ_∞ [°C]	
			$\mu = 0.15$	$\mu = 0.3$
10	0.5	3.32	109	218
10	1.0	6.64	218	435
10	1.5	9.95	327	653
20	0.5	2.35	77	154
20	1.0	4.69	154	308
20	1.5	7.04	231	462
30	0.5	1.92	63	126
30	1.0	3.83	126	251
30	**1.3**	**4.98**	**163**	**327**
30	1.5	5.75	189	377
50	0.5	1.48	48	97
50	1.0	2.97	97	195
50	1.5	4.45	146	292

ellipse a and b are in the range of 6–10 mm, with the maximum Hertz pressure $p_0 \approx 800$ MPa. With $a = 6$ mm, the Johnson number is J ≈ 5, s. Table 1. The coefficient of friction is assumed to be $\mu = 0.3$. If the wheel and rail are initially at ambient temperature, i.e. at the beginning of these operating conditions (Fig. 14), the shakedown limit of the rail decreases to 68% compared to the case without consideration of thermal stresses (Fig. 1) and the maximum contact temperature is 207 °C. For continuous operation, the wheel temperature increases and the shakedown limit of the rail is reduced to 50% only, s. Fig. 15. The steady-state temperature of the wheel is then 328 °C.

With these operating conditions, the shakedown limit of the wheel is almost uninfluenced by the thermal stresses. It can even be slightly higher than without thermal stresses since the resulting stress level at the surface is reduced by the additional thermal stresses. At higher values of the Johnson number J, the shakedown limit of the wheel becomes also considerably decreased, Figs. 16 and 17. If the wheel has reached the limit temperature Θ_∞ at very high values of J, the elastic and the shakedown limits of the rail are only half as high as those for the wheel, Fig. 17. This is due to the pure thermal stresses in the rail which are twice as high as those in the wheel. The rail in the case of driving therefore suffers most from thermal stresses, especially at high initial wheel temperatures.

When a locomotive is pulling a train, the tractive forces are transmitted only by the wheels of the locomotive. This is the normal state for long periods of operation, e.g. for high speed traffic

or climbing up hills. In contrast, all wheels of the train participate in braking. Therefore it seems reasonable that high tractive forces and thermal stresses should be expected mostly in the driving case. The rail is subjected to much higher stresses in this case. It is even possible that repeated plastic flow occurs in the rail even though the wheel is still far away from the onset of yield, Fig. 18. This can cause structural changes in the rail material as well as rail damage, as described in [6]. The maximum contact temperatures are not much above 300 °C for typical wheel/rail operating conditions and should not be able to cause thermally induced phase transformations. Nevertheless, the resulting thermal stresses have a significant influence on the material of the wheels and rails.

8 Conclusions

Friction between wheel and rail results in considerable contact temperatures and gives rise to severe thermal stresses at the surfaces of wheels and rails. An approximate analytical solution has been presented for the line contact. If the wheel and rail are initially at ambient temperature, all influence parameters for the thermal stresses can be combined into a single non-dimensional parameter, the Johnson number J, Eq. (28). The increased bulk temperature of the wheel after some long period of constant operation has also been taken into account. The upper limit of the wheel temperature depends on the heat flow from the hot wheel into the cold rail through the contact patch. The initial relative temperature $\tilde{\Theta}_0$ of the wheel, Eq. (15), is the second non-dimensional parameter for the consideration of thermal stresses in rolling contact.

The results presented in this paper show that there is a significant influence of thermal stresses on the elastic limit and the shakedown limit in a wheel/rail contact. If the wheel is initially at ambient temperature, the components of mechanical and thermal stresses are partly equal in the wheel and the rail, but their reverse direction results in different levels of equivalent stress. With an increased initial temperature of the wheel, the thermal stresses are even higher in the rail, whereas they get reduced in the wheel. The worst situation for the rail is always in the case of driving. Its elastic and shakedown limits can be reduced by a factor two as compared to the wheel.

Although the model of an infinite cylinder subjected to normal and tangential loads is only a rough approximation of the real wheel/rail contact, the results for three-dimensional contact problems (elliptical area of contact) should be similar. In the case of rolling contact with pure mechanical load, i.e. without thermal stresses, this has already been shown in [3, 18].

The real behaviour of rail steel should be considered with a more realistic model. Lately, a Chaboche model was used for the numerical investigation of plastic deformations on rail surfaces subjected to cyclic loading, [25]. The finite element solution presents only results for special examples. The temperature dependence of material parameters should be taken into account in a more detailed investigation.

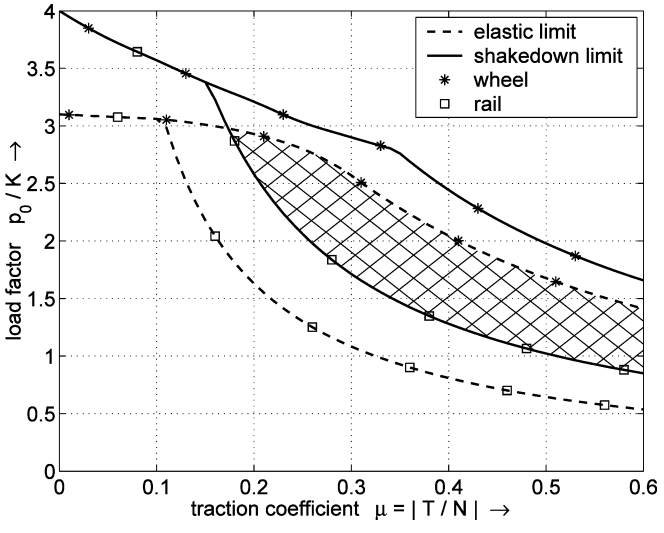

Fig. 18. Shakedown map in the case of driving; Johnson number J = 5, initial relative wheel temperature $\tilde{\Theta}_0 = 0.5$. The hatched section: the shakedown limit of the rail exceeded, the wheel below the elastic limit

References

1. **Hertz, H.:** Über die Berührung fester elastischer Körper. J. für die reine und angewandte Mathematik 92 (1881) 156–171
2. **Johnson, K.L.:** A shakedown limit in rolling contact. Proc of the 4th US National Congress of Applied Mechanics (1962) 971–975
3. **Johnson, K.L.; Jefferis, J.A.:** Plastic flow and residual stresses in rolling and sliding contact. Proc Institution of Mechanical Engineers, Symposium on Rolling Contact Fatigue (1963) 50–61
4. **Melan, E.:** Der Spannungszustand eines "Mises-Hencky'schen" Kontinuums bei veränderlicher Belastung. Sitzungsberichte der Akademie der Wissenschaften in Wien 147 (1938) 73–87
5. **Merwin, J.E.; Johnson, K.L.:** An analysis of plastic deformation in rolling contact. Proc. Institution of Mechanical Engineers 177(25) (1963) 676–690
6. **Pointner, P.:** Auswirkungen des Rad-Schiene-Kontaktes auf Werkstoffwahl und Fahrweggüte. EI – Der Eisenbahningenieur 51(9) (2000) 122–126
7. **Bhargava, V.; Hahn, G.T.; Rubin, C.A.:** An elastic-plastic finite element model of rolling contact I: Analysis of single contacts. Trans ASME J Appl Mech 52 (1985) 67–74
8. **Bhargava, V.; Hahn, G.T.; Rubin, C.A.:** An elastic-plastic finite element model of rolling contact II: Analysis of repeated contacts. Trans ASME J Appl Mech 52 (1985) 75–82
9. **Fermér, M.:** Railway wheelsets – theory, experiments and design considering temperatures, stresses and deformations as induced by bracking loads and contact forces. (PhD thesis) Göteborg, Chalmers University of Technology, 1993
10. **Johnson, M.R.; Welch, R.E.; Yeung, K.S.:** Analysis of thermal stresses and residual stress changes in railroad wheels caused by severe drag braking. Trans ASME J Eng Indust 99 (1977) 18–23
11. **Moyar, G.J.; Stone, D.H.:** An analysis of the thermal contributions to railway wheel shelling. Wear 144 (1991) 117–138
12. **Gupta, V.; Hahn, G.T.; Bastias, P.C.; Rubin, C.A.:** Thermal-mechanical modelling of the rolling-plus-sliding with frictional heating of a locomotive wheel. Trans ASME J Eng Indust 117 (1995) 418–422
13. **Barber, J.R.:** Thermoelastic displacements and stresses due to a heat source moving over the surface of a half plane. Trans ASME J Appl Mech 51 (1984) 636–640
14. **Fischer, F.D.; Werner, E.; Yan, W.:** Thermal stresses for frictional contact in wheel-rail systems. Wear 211 (1997) 156–163
15. **Hills, D.A.; Nowell, D.; Sackfield, A.:** The state of stress induced by cylindrical sliding contacts with frictional heating. Int J Mech Sci 32(9) (1990) 767–778
16. **Ponter, A.R.S.; Fuschi, P.; Engelhardt, M.:** Limit analysis for a general class of yield conditions. Eur J Mech A/Solids 19 (2000) 401–421
17. **Ponter, A.R.S.; Engelhardt, M.:** Shakedown limits for a general yield condition: implementation and application for a Von Mises yield condition. Eur J Mech A/Solids 19 (2000) 423–445
18. **Johnson, K.L.:** Contact Mechanics. Cambridge, Cambridge University Press. 1985
19. **Knothe, K.; Liebelt, S.:** Determination of temperatures for sliding contact with applications for wheel-rail systems. Wear 189 (1995) 91–99
20. **Ertz, M.; Knothe, K.:** A comparison of analytical and numerical methods for the calculation of temperatures in wheel/rail contact. Wear 253(3–4) (2002) 498–508
21. **Knothe, K.; Wille, R.; Zastrau, B.W.:** Advanced contact mechanics – road and rail. Vehicle Syst Dyn 35(4–5) (2001) 361–407
22. **Carslaw, H.C.; Jaeger, J.C.:** Conduction of Heat in Solids. Oxford, Oxford University Press. 1959
23. **Ertz, M.; Bucher, F.:** Improved creep force model for wheel/rail contact considering roughness and temperature. In: True, H. (ed.) The Dynamics of Vehicles on Road and Tracks. Proc. of the 17th IAVSD Symposium, DTU (2001) Lyngby (Copenhagen), Denmark. In press
24. **Schouten, M.J.W.:** Einfluß elastohydrodynamischer Schmierung auf Reibung, Verschleiß und Lebensdauer von Getrieben. (PhD thesis). Technische Hogeschool Eindhoven, 1973
25. **Böhmer, A.; Klimpel, T.:** Plastic deformation of corrugated rails – a numerical approach using material data of rail steel. Wear 253(1–2) (2002) 150–161